Small

NANO · MICRO small
www.small-journal.com

RESEARCH ARTICLE

About Carrier's Self-Trapping and Dynamical Rashba Splitting in the 2D Hybrid Perovskite $(BA)_2(MA)_2Pb_3I_{10}$

Weiyan Qi[1] | Stefano Ponzoni[1] | Guénolé Huitric[1] | Vitaly Gorelov[1] | Ashim Pramanik[1] | Yannis Laplace[1] | Marino Marsi[2] | Evangelos Papalazarou[2] | Sebastian F. Maehrlein[3,4,5] | Emmanuelle Deleporte[6] | Nitin Mallik[7] | Amina Taleb-Ibrahimi[7] | Azzedine Bendounan[7] | Kaibo Zheng[8,9] | Tönu Pullerits[9] | Luca Perfetti[1]

[1]Laboratoire des Solides Irradiés, CEA/DRF/IRAMIS, CNRS, Ecole Polytechnique, Institut Polytechnique de Paris, Palaiseau, France | [2]Laboratoire de Physique des Solides, Université Paris-Saclay, CNRS, Orsay, France | [3]Department of Physical Chemistry, Fritz Haber Institute of the Max Planck Society, Berlin, Germany | [4]Institute of Radiation Physics, Helmholtz-Zentrum Dresden-Rossendorf, Dresden, Germany | [5]Institute of Applied Physics, Dresden University of Technology, Dresden, Germany | [6]Université Paris-Saclay, ENS Paris-Saclay, CentraleSupélec, CNRS, Lumière, Matière et Interfaces (LuMIn) Laboratory, Gif-sur-Yvette, France | [7]Société civile Synchrotron SOLEIL, L'Orme des Merisiers, Saint-Aubin - BP 48, GIF-sur-YVETTE, France | [8]Department of Chemistry, Technical University of Denmark, Kongens Lyngby, Denmark | [9]Chemical Physics and NanoLund, Lund University, Lund, Sweden

Correspondence: Luca Perfetti (luca.perfetti@polytechnique.edu)

Received: 16 September 2025 | **Revised:** 13 January 2026

Keywords: 2D perovskite | band structure | exciton | Rashba | self trapping

ABSTRACT

Time- and Angle-Resolved Photoelectron Spectroscopy (tr-ARPES) is employed to monitor photoexcited electrons in the 2D hybrid perovskite $(BA)_2(MA)_2Pb_3I_{10}$. Photoelectron intensity maps are in good agreement with ab-initio calculations of the band structure. The effective mass is $-0.18 \pm 0.02m_0$ and $0.12 \pm 0.02m_0$ for holes and electrons, respectively. In the photoexcited state, spin-orbit splitting of the conduction band cannot be resolved. This sets the upper bound of photoinduced Rashba coupling to $\alpha_C < 2.5$ eVÅ. The correlated electron-hole plasma evolves in Wannier excitons with Bohr radius of 2.8 nm, while no sign of self-trapping in small polarons is found within the investigated time window of up to 120 ps following photoexcitation.

1 | Introduction

Dynamical disorder refers to large fluctuations of the local atomic structure within the crystal. In the case of hybrid perovskites, such a phenomenon could generate ferroelectric domains [1] and significantly affect the electronic states [2, 3]. For example, dynamical disorder could favor the self-trapping of carriers in polaronic states [4]. Alternatively, the local breakdown of inversion symmetry [5] may lift spin degeneracy at the band extrema, leading to counterrotating spin textures of electronic states with spin-momentum locking [6]. If experimentally verified, these effects would have important implications for optoelectronic properties of such hybrid materials. Despite the numerous reports, the subject is still a matter of debate, both experimentally and theoretically.

An ideal technique to explore the structure of electronic states out of equilibrium is time and Angle Resolved Photoelectron Spectroscopy (tr-ARPES) [7–9]. In the case of a semiconductor, a visible pump laser excites electrons from the valence to the conduction band, while an ultraviolet probe pulse induces the emission of photoelectrons. An analyzer provides instantaneous snapshots of the electronic states as function of energy and wavevector [9]. Here we employ both ARPES and tr-ARPES to map the electronic states of the 2D hybrid perovskite $(BA)_2(MA)_2Pb_3I_{10}$. As shown in Figure 1a, the structure corresponds to the $n = 3$ variant of the Ruddlesden-Popper series $(BA)_2(MA)_{n-1}Pb_nI_{3n+1}$. It can be regarded as three layers of $[PbI_6]$ octahedral sheets, intercalated by MA cations and sandwiched by two layers of butylammonium ligands [10]. This arrangement gives rise to multiple-quantum-well structures, in which the

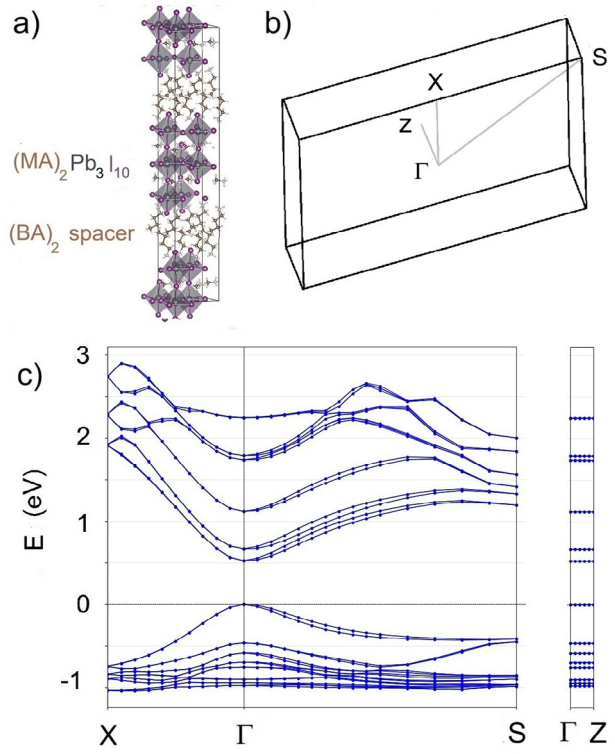

FIGURE 1 | a) Schematic structure of the 2D perovskite $(BA)_2(MA)_{n-1}Pb_nI_{3n+1}$ with $n = 3$. b) Brillouin zone of the orthorhombic unit cell. c) Dispersion of electronic states along the $\Gamma - X$ and $\Gamma - S$ and $\Gamma - Z$symmetry directions, obtained with PBE-DFT and including spin-orbit coupling.

inorganic slabs serve as the potential well while the organic layers function as the potential barriers [11]. Note that $(BA)_2(MA)_2Pb_3I_{10}$ crystallizes in the noncentrosymmetric space group $C2cb$ [10], meaning that $[PbI_6]$ octahedra reorientation develops a net dipole moment within the unit cell. Figure 1b shows the surface Brillouin zone of the orthorhombic unit cell (black lines) and of a hypothetical unit cell obtained by neglecting octahedra distortions (blue lines). The Valence Band Maximum (VBM) is located at the Γ' point, while a weak VBM replica [12] is backfolded at Γ by lattice distortions.

2 | Results

We performed PBE-DFT calculations for the experimentally detetermined structure [10] of $(BA)_2(MA)_2Pb_3I_{10}$. The computations employed a plane-wave energy cutoff of 40 Hartree and a 4×2×4 Monkhorst-Pack k-point grid. Spin–orbit coupling was included via fully relativistic pseudopotentials [13, 14]. Figure 1c shows the electronic band structure calculated along the high-symmetry path X(1/2,0,0) – Γ(0,0,0) – S(1/2,0,1/2) and in the out of plan direction $\Gamma(0,0,0) - Z(0,1/2,0)$. The PBE-DFT bandgap at the Γ-point is found to be 0.52 eV, significantly lower than the experimental value of 2.1 eV [10]. This discrepancy is a well-known limitation of DFT calculations, which consistently underestimate bandgap values. Theoretical estimate of effective masses are obtained by fitting the band dispersion along the $\Gamma - X$ path close to the band edges, resulting in $-0.16 \pm 0.01m_0$ and $0.12 \pm 0.01m_0$ for holes and electrons, respectively. These values are somewhat larger than reported PBEsol-DFT [10, 15] calculations of the in-plane averaged effective masses. We have performed a PBEsol-DFT calculations and have found a ≅ 5 – 10% reduction of the hole and electron effective masses giving a good agreement with Stoumpos et al. [10] (see Figure S5, Supporting Information). The electronic bands exhibit complex Spin-Orbit splitting (SO), that varies significantly with the crystallographic direction. As shown in Figure 1c, the SO is negligible along the $\Gamma - X$ direction while attains the maximal value $\Delta E =$ 80 meV along the $\Gamma - S$ direction. Such anisotropic SO [16] mainly originates from in-plane asymmetric tilting of adjacent metal halide octahedra. A small wavevector expansion along the $\Gamma - S$ direction theoretically provides a Rashba parameter $\alpha_C = 0.35$ eVÅ for the electronic states of the conduction band. This value is consistent with the equilibrium SO splitting calculated by Jana et al. for similar compounds [16] and is one order of magnitude smaller than the SO splitting predicted by Etienne et al. [6] for a fluctuating lattice.

Bulk single crystals of $(BA)_2(MA)_2Pb_3I_{10}$ were grown by the temperature gradient method [17]. ARPES maps have been acquired on the TEMPO beamlime of Synchrotron Soleil, with a hemispherical analyzer MBS A-1 equipped with vacuum tunable lens axis. The photon beam is centered at 55 eV, horizontally polarized and focused down to 100 × 300 microns. Single crystals of $(BA)_2(MA)_2Pb_3I_{10}$ have been cleaved in ultra-high vacuum conditions and measured at 80 K. The natural cleavage plane lies in the buffer layer of the BA ligands, exposing a highly passivated surface. However two-dimensional hybrid perovskites can be easily damaged by XUV photons, so that no ARPES data have ever been reported yet. In this work, we have successfully overcome this limitation by implementing a rapid rastering acquisition mode for ARPES and tr-ARPES, enabling the direct measurement of the band structure in these materials (details are given in Supporting Information).

As shown in Figure 2a the electronic states disperse along the $\Gamma - X - \Gamma'$ direction, reaching the VBM at Γ'. By integrating the intensity map around the VBM, we obtain a Momentum Distribution Curve (MDC) exhibiting peaks at Γ'. Also note that a weak, folded replica is generated at Γ by octahedral distortions. Instead, by integrating the intensity map around Γ' we obtain an Energy Distribution Curve (EDC). Of the 400 meV peak broadening, a contribution of $2\Sigma_I = 100$ meV can be ascribed, via *ab-initio* simulations, to the intrinsic electron-phonon linewidth [18], while the remaining 300-meV contribution is likely to be dominated by inhomogeneous and extrinsic factors.

The PBE-DFT calculations (dashed white line in Figure 2a) are consistent, within the experimental spectral broadening, to the ARPES intensity map. By fitting EDCs we obtain $m_V = -0.18 \pm 0.02m_0$. This effective mass is similar to the recently reported values in $(MA)PbI_3$ [12] or $CsPbBr_3$ [19, 20]. We stress that $m_V = -0.18m_0$ should be considered as a ***bare*** mass value, i.e., not accounting for the renormalization effects of electron-phonon coupling [21]. The reason is that ARPES intensity maps vary over an energy interval that is an order of magnitude larger than the energy scale of the longitudinal optical phonons (i.e., $\hbar\Omega \cong 20$ meV) [18].

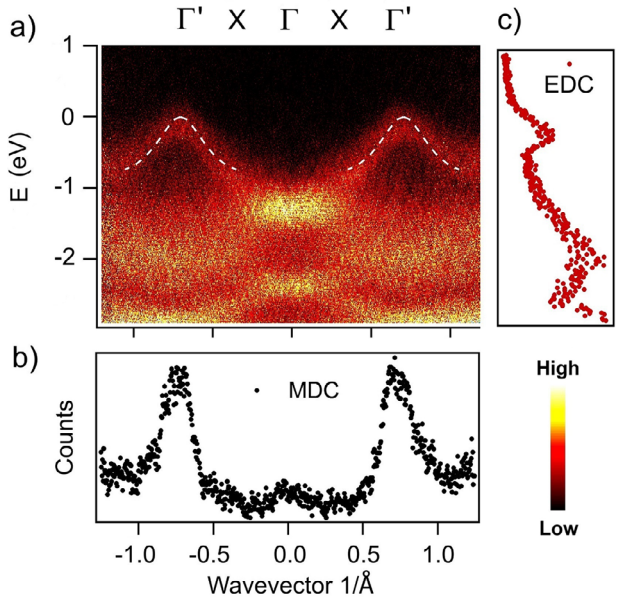

FIGURE 2 | a) Valence band dispersion acquired along the $\Gamma - X - \Gamma'$ direction. Energies have been referred with respect to the valence band maximum. The white dashed line is the valence band dispersion predicted by the *ab-initio* calculations of Figure 1c. b) Momentum Distribution Curve (MDC) extracted by integrating in an energy interval of 50 meV around the Valence Band Maximum (VBM). c) EDC extracted by integrating in a wavevector interval of 0.05 $Å^{-1}$ around Γ'.

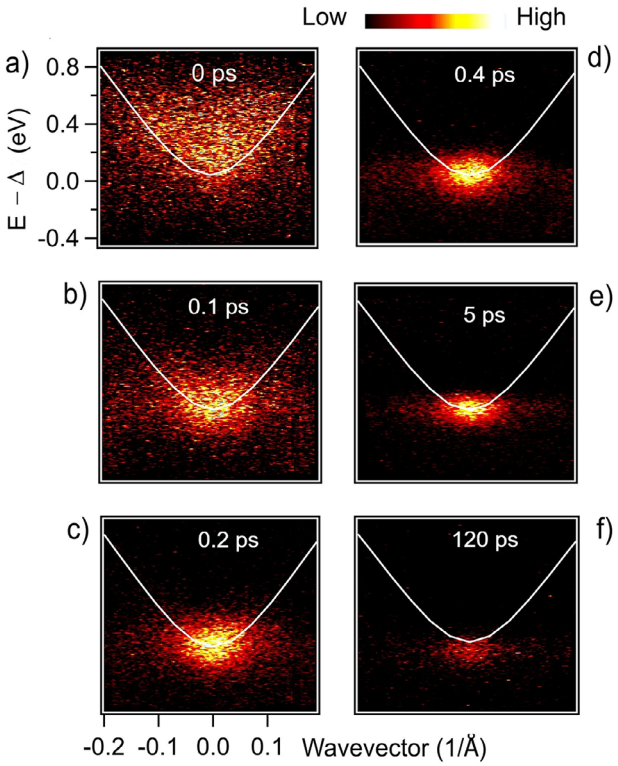

FIGURE 3 | a–f) Time resolved ARPES map along $\Gamma - X$ for different pump probe delays. With respect to the valence band map, the energy scale has been shifted by the optical gap Δ. The white line is the conduction band dispersion predicted by *ab-initio* calculations of Figure 1c.

The dynamics of electronic states in the conduction band is obtained via a two photon process. The probe beam, is horizontally polarized, has photon energy of 6.2 eV and is focused down to 100 × 100 microns. The pump beam has photon energy of 3.1 eV and has incident fluence of 10 μJ cm^{-2}, corresponding to photoexcitation density $\rho \cong 1 \times 10^{12}$ cm^{-2}. The cross correlation between pump and probe has a Full Width Half Maximum of roughly 120 fs [22]. Single crystals of $(BA)_2(MA)_2Pb_3I_{10}$ are cleaved at 300 K in ultra-high vacuum conditions and measured at temperature below 140 K. Also in this case, the sample has been rastered during data acquisition (see also Supporting Information).

Figure 3a–f shows the tr-ARPES intensity maps acquired along the $\Gamma - X$ direction for different pump-probe delays. The electrons are highly excited by the 3.1 eV pump beam and partially relax within the duration of the pump pulse. At zero delay (see Figure 3a), the transient signal extends up to 0.5 eV above the Conduction Band Minimum (CBM) and it is widely distributed at energies greater than the *ab-initio* calculated dispersion of the conduction band (white line in Figure 3). The electron effective mass, which has never been experimentally reported in any hybrid perovskite, is determined here to be $m_C = 0.12 \pm 0.2 m_0$.

Figure 3b shows that hot electrons underwent strong energy relaxation as early as 0.1 ps after photoexcitation, confirming the occurrence of strong inelastic scattering. Similar findings have been previously observed in 3D hybrid perovskite $(MA)PbI_3$ [23, 24] and in four cations mixtures [25, 26]. In all these cases, the energy relaxation mainly occur by collision with stretching and libration modes of the $[PbI_6]$ octahedra [18]. The reported value of inverse quasiparticles lifetime $2\Sigma_I \cong 100$ meV [18] leads to cooling rate of $2\Sigma_I\Omega$, so that hot electrons with average excess energy $\langle E \rangle = 0.5$ eV are expected to relax in $\cong \langle E \rangle / (2\Sigma_I\Omega) \cong 0.15$ ps [9]. This prediction is in line with tr-ARPES maps of Figure 3a–c.

3 | Discussion

After 0.4 ps (see Figure 3d) the electrons have relaxed, either forming a ionized carriers near to the conduction band minimum [27], or already forming hot excitons. The second hypothesis is more likely as long as the photoexcitation density is not large enough to destabilize the bound el-h states. To prove that excitons are stable at our photoexcitation density, we monitored the tr-ARPES intensity while scanning a pump beam across the optical bandgap. Figure 4 in the Supporting Information shows an exciton resonance peaking at an optical gap of 2.1 eV. The resonance signal corresponds to the photoexcitation density ρ, confirming the possible formation of excitons also for the above gap pumping and at early delay time (0.4 ps). As can be seen in Figure 3d–f, the ARPES intensity decreases substantially (more precisely a factor 3) when moving from a delay of 0.4–120 ps. Unlike in the case of 3D perovskites [23], the reduced signal intensity is entirely due to carrier recombination. The reason is that the BA ligand hinders the interlayer hopping of electrons, preventing the carrier diffusion from the surface to the bulk. Notice that the ARPES signal of Figure 3d–f is sharply peaked at the center of the Brillouin Zone and shifts to lower energy by about 60 meV at delay times of 120 ps (see also

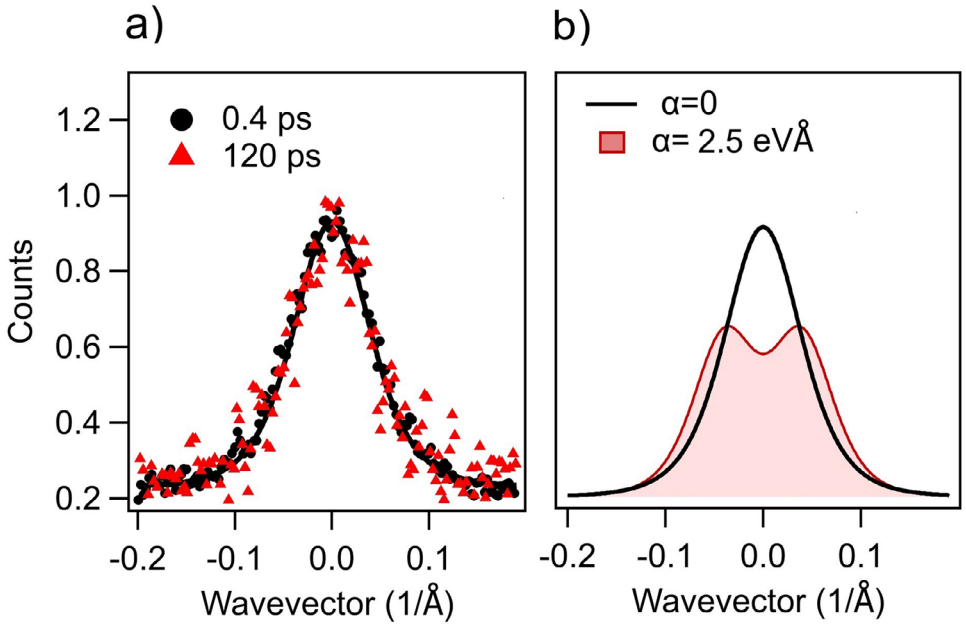

FIGURE 4 | Momentum Distribution Curves extracted at the CBM for delay times of 0.4 ps (dark circles) and 120 ps (red triangles). The MDCs have been renormalized to the maximum value and fit (solid line) with the model function $|\phi(k)|^2$ described in the text. b) Best fitting function of the MDC (black curve) and model MDC curve assuming $\alpha_C = 2.5$ eVÅ(shadow pink area).

Figure S3, Supporting Information). Such an energy shift suggests the evolution from dense and hot exciton ensemble (at 0.4 ps) to a low density exciton gas (at 120 ps).

Since our excitation is not resonant, the ARPES intensity maps in Figure 3d–f do not exhibit the negative exciton dispersion that has been reported in transition metal dichalcogenides [28, 29]. This Floquet dressing is not always observed [30–32], because is enhanced by resonant excitation conditions and may depend on specific material system. Theoretical studies also indicate that, in the case of excitation above the gap, the signal is dominated the thermal and incoherent population of excitons with finite center-of-mass momentum [33].

Further conclusions can be drawn from the distribution of spectral weight in wavevector space. Figure 4a shows the MDCs extracted by integrating the ARPES intensity map in an energy interval of 0.1 eV around the CBM, at a delay time of 0.4 ps (dark circles) and 120 ps (red triangles). The two MDCs can be nicely superimposed by applying a relative multiplication factor. They both peak at Γ and can be fitted by the function $|\phi(k)|^2 = 1/(1 + a_0^2 k^2/4)^3$ convoluted by the wavevector resolution of the setup. Here $\phi(k)$ is the 2D Fourier transform of $\phi(r) \propto \exp(-2r/a_0)$, namely the model function of a two dimensional exciton with Bohr radius a_0. The simple 2D hydrogenic model yields $a_0 \cong 2-4$ nm when considering the exciton effective mass $|m_C m_V|/(|m_C| + |m_V|)$, together with an effective in-plane dielectric constant $\varepsilon \cong 3-5$. The fitting of the experimental data results in $a_0 = 2.8$ nm, which indeed falls within the expected range. Furthermore, the exciton extension $\sqrt{\langle r^2 \rangle} = \sqrt{3/2}a_0 = 3.4$ nm is in good agreement with the spectroscopy of Landau levels at high magnetic fields [34].

The area covered by $\phi(r)$ (i.e., $\pi\langle r^2 \rangle = 36$ nm^2) contains 45 unit cells, therefore excluding the self-trapping of excitons in polaronic cages having the size of inter-ionic distance. This result is important for the ongoing debate about whether excitons are trapped extrinsically or intrinsically in these kinds of materials [35]. Indeed, the formation of localized, Frenkel-like, excitons would lead to a dispersionless state across the wave-vector window considered here. We conclude that the subgap emission observed in $(BA)_2(MA)_{n-1}Pb_nI_{3n+1}$ [36] are likely due to exciton trapping by a small concentration of extrinsic defects, which may be visible in integrated photo-luminescence but is irrelevant in a tr-ARPES experiment.

The last topic to discuss is dynamical Spin Orbit splitting (SO). Transient spin polarization of electronic states with $\alpha_C > 10$ eVÅ have been proposed by theoretical simulations [6] and claimed by the spectral analysis of two photon absorption [37]. The proposed conjecture is that ionic lattice motion and dynamical formation of fluctuating ferroelectric domains could locally increase the SO splitting. This effect could be even boosted if excited electrons would self trap in polaronic states. However, designing experiments that could ambiguously estimate the dynamical SO is especially challenging. For example, the difference in threshold energy between one-photon and two-photon absorption could be dominated by the optical selection rules of the exciton lines rather than SO splitting. The tr-ARPES is a far more direct approach for monitoring the potential presence of dynamical Rashba spitting. Figure 4b plots the fitting curve of the experimental MDCs (black line), and the MDC model assuming $\alpha_C = 2.5$ eVÅ (pink shadow area). The absence of a double peak in the experimental MDC let us conclude that $\alpha_C < 2.5$ eVÅ. Same result is obtained analyzing data acquired along the $\Gamma - S$ direction. This upper bound of α_C is consistent with our *ab-initio* calculations and it excludes that fluctuating ferroelectric domains can generate a dynamical Rashba splitting 10 times larger than the frozen lattice value.

4 | Conclusions

In conclusion, ARPES and TR-ARPES experiments on 2D hybrid Perovkistes enable us to visualise the dispersion of electronic states within the valence and conduction bands. This challenging measurement has only been possible here thanks to sample rastering during data acquisition. Our intensity maps show experimental effective masses in good agreement with first-principles calculations. First, excited electrons relax to the bottom of the conduction band, and then they form bound states with the underlying holes. The wavevector tomography of the resulting wavefunction is compatible with Wannier excitons with a Bohr radius of 2.8 nm. No evidence of self-trapping is observed until 120 ps after photoexcitation. Moreover, a thorough analysis of the momentum distribution curve also excludes that fluctuating ferroelectric domains can give rise to dynamic Rashba splitting of very large amplitude.

Acknowledgments

We acknowledge financial support of the 2D-HYPE project from the Agence Nationale de la Recherche (ANR, Nr. ANR 21-CE30-0059), of the Deutsche Forschungsgemeinschaft (DFG, German Research Foundation, Nr. 490867834), of the MINTOAURE project (ANR A-22-PETA-0015) and of the Région Ile de France via (FemtoARPES2.0 project N. EX079194). Weiyan Qi thanks the China Scholarship Council (CSC). Computational time was granted by GENCI (Project No. 544).

Conflicts of Interest

The authors declare no conflict of interest.

Data Availability Statement

The data that support the findings of this study are available from the corresponding author upon reasonable request.

References

1. J. M. Frost, K. T. Butler, F. Brivio, C. H. Hendon, M. van Schilfgaarde, and A. Walsh, "Atomistic Origins of High-Performance in Hybrid Halide Perovskite Solar Cells," *Nano Letters* 14 (2014): 2584.

2. D. Ghosh, E. Welch, A. J. Neukirch, A. Zakhidov, and S. Tretiak, "Polarons in Halide Perovskites: A Perspective," *Journal of Physical Chemistry Letters* 11 (2020): 3271.

3. P. Nandi, S. Shin, H. Park, Y. In, et al., "Large and Small Polarons in Highly Efficient and Stable Organic-Inorganic Lead Halide Perovskite Solar Cells: A Review," *Solar: Rapid Research Letters* 8 (2024): 2400364.

4. A. J. Neukirch, W. Nie, J.-C. Blancon, et al., "Polaron Stabilization by Cooperative Lattice Distortion and Cation Rotations in Hybrid Perovskite Materials," *Nano Letters* 16 (2016): 3809.

5. J. M. Urban, M. S. Spencer, M. Frenzel, et al., "THz-Driven Coherent Phonon Fingerprints of Hidden Symmetry Breaking in 2D Layered Hybrid Perovskites," https://arxiv.org/abs/2503.02529 (2025).

6. T. Etienne, E. Mosconi, and F. De Angelis, "Dynamical Origin of the Rashba Effect in Organohalide Lead Perovskites: A Key to Suppressed Carrier Recombination in Perovskite Solar Cells?," *Journal of Physical Chemistry Letters* 7 (2016): 1638.

7. Y. Ohtsubo, J. Mauchain, J. Faure, et al., "Giant Anisotropy of Spin-Orbit Splitting at the Bismuth Surface," *Physical Review Letters* 109 (2012): 226404.

8. J. Dong, D. Shin, E. Pastor, et al., "Electronic Dispersion, Correlations and Stacking in the Photoexcited State of 1T-TaS2," *2D Materials* 10 (2023): 045001.

9. Z. Chen, C. Giorgetti, J. Sjakste, et al., "Ultrafast Electron Dynamics Reveal the High Potential of InSe for Hot-Carrier Optoelectronics," *Physical Review B* 97 (2018): 241201.

10. C. C. Stoumpos, D. H. Cao, D. J. Clark, et al., "Ruddlesden–Popper Hybrid Lead Iodide Perovskite 2D Homologous Semiconductors," *Chemistry of Materials* 28 (2016): 2852.

11. Y. Chen, Y. Sun, J. Peng, J. Tang, K. Zheng, and Z. Liang, "2D Ruddlesden–Popper Perovskites for Optoelectronics," *Advanced Materials* 30 (2018): 1703487.

12. J. Park, S. Huh, Y. W. Choi, et al., "Visualizing the Low-Energy Electronic Structure of Prototypical Hybrid Halide Perovskite Through Clear Band Measurements," *ACS Nano* 18 (2024): 7570.

13. J. P. Perdew, K. Burke, and M. Ernzerhof, "Generalized Gradient Approximation Made Simple," *Physical Review Letters* 77 (1996): 3865.

14. M. J. van Setten, M. Giantomassi, E. Bousquet, et al., "The PseudoDojo: Training and Grading a 85 Element Optimized Norm-Conserving Pseudopotential Table," *Computer Physics Communications* 226 (2018): 39.

15. N. Zibouche and M. S. Islam, "Structure–Electronic Property Relationships of 2D Ruddlesden–Popper Tin- and Lead-Based Iodide Perovskites," *ACS Applied Materials & Interfaces* 12 (2020): 15328.

16. M. K. Jana, R. Song, Y. Xie, et al., "Structural Descriptor for Enhanced Spin-Splitting in 2D Hybrid Perovskites," *Nature Communications* 12 (2021): 4982.

17. W. Lin, M. Liang, Y. Niu, et al., "Combining Two-Photon Photoemission and Transient Absorption Spectroscopy to Resolve Hot Carrier Cooling in 2D Perovskite Single Crystals: The Effect of Surface Layer," *Journal of Materials Chemistry C* 10 (2022): 16751.

18. A. D. Wright, C. Verdi, R. L. Milot, et al., "Electron–Phonon Coupling in Hybrid Lead Halide Perovskites," *Nature Communications* 7 (2016): 11755.

19. M. Puppin, S. Polishchuk, N. Colonna, et al., "Evidence of Large Polarons in Photoemission Band Mapping of the Perovskite Semiconductor CsPbBr3," *Physical Review Letters* 124 (2020): 206402.

20. M. Sajedi, M. Krivenkov, D. Marchenko, et al., "Is There a Polaron Signature in Angle-Resolved Photoemission of CsPbBr3?," *Physical Review Letters* 128 (2022): 176405.

21. S. L. Perfetti, G. Mitrovic, M. Margaritondo, et al., "66 Mobile Small Polarons and the Peierls Transition in the Quasi-One-Dimensional Conductor K0.3MoO3," *Physical Review B* 66 (2002): 075107.

22. J. Faure, J. Mauchain, E. Papalazarou, et al., *Review of Scientific Instruments* 83 (2012): 043109.

23. Z. Chen, M.-I. Lee, Z. Zhang, et al., "Time-Resolved Photoemission Spectroscopy of Electronic Cooling and Localization in ch3nh3pbi3 Crystals," *Physical Review Materials* 1 (2017): 045402.

24. M. Cherasse, J. Dong, G. Tripp'e-Allard, et al., "Electron Dynamics in Hybrid Perovskites Reveal the Role of Organic Cations on the Screening of Local Charges," *Nano Letters* 22 (2022): 2065.

25. E. Jung, K. Budzinauskas, S. Oz, et al., "Femto- to Microsecond Dynamics of Excited Electrons in a Quadruple Cation Perovskite," *ACS Energy Letters* 5 (2020): 785.

26. M. Cherasse, N. Heshmati, J. M. Urban, et al., "Enhanced Lattice Coherences and Improved Structural Stability in Quadruple A-Site Substituted Lead Bromide Perovskites," *Small* 21 (2025): 2500977.

27. V. Gosetti, J. Cervantes-Villanueva, S. Mor, et al., "Unveiling the Exciton Formation in Time, Energy and Momentum Domain in Layered van der Waals Semiconductors," *Progress in Surface Science* 100 (2025): 100777.

28. M. K. L. Man, J. Mad'eo, C. Sahoo, et al., "Experimental Measurement of the Intrinsic Excitonic Wave Function," *Science Advances* 7 (2021): eabg0192.

29. S. Dong, M. Puppin, T. Pincelli, et al., "Direct Measurement of Key Exciton Properties: Energy, Dynamics, and Spatial Distribution of the Wave Function," *Natural Sciences* 1 (2021): e10010.

30. J. Mad'eo, M. K. L. Man, C. Sahoo, et al., "Directly Visualizing the Momentum-Forbidden Dark Excitons and Their Dynamics in Atomically Thin Semiconductors," *Science* 370 (2020): 1199.

31. D. Schmitt, J. P. Bange, W. Bennecke, et al., "Formation of Moir'e Interlayer Excitons in Space and Time," *Nature* 608 (2022): 499.

32. R. Wallauer, R. Perea-Causin, L. Müunster, et al., "Momentum-Resolved Observation of Exciton Formation Dynamics in Monolayer ws_2," *Nano Letters* 21 (2021): 5867.

33. D. Christiansen, M. Selig, E. Malic, R. Ernstorfer, and A. Knorr, "Theory of Exciton Dynamics in Time-Resolved Arpes: Intra- and Intervalley Scattering in Two-Dimensional Semiconductors," *Physical Review B* 100 (2019): 205401.

34. M. Dyksik, S. Wang, W. Paritmongkol, et al., "Tuning the Excitonic Properties of the 2D (pea)2(ma)n-1pbni3n+1 Perovskite Family via Quantum Confinement," *Journal of Physical Chemistry Letters* 12 (2021): 1638.

35. M. D. Smith and H. I. Karunadasa, "White-Light Emission from Layered Halide Perovskites," *Accounts of Chemical Research* 51 (2018): 619.

36. J. Li, J. Wang, J. Ma, et al., "Self-Trapped State Enabled Filterless Narrowband Photodetections in 2D Layered Perovskite Single Crystals," *Nature Communications* 10 (2019): 806.

37. E. Lafalce, E. Amerling, Z.-G. Yu, P. C. Sercel, L. Whittaker-Brooks, and Z. V. Vardeny, "Rashba Splitting in Organic–Inorganic Lead–Halide Perovskites Revealed Through Two-Photon Absorption Spectroscopy," *Nature Communications* 13 (2022): 483.

Supporting Information

Additional supporting information can be found online in the Supporting Information section.

Supporting Information